Enhancement of 250-MHz quantitative acoustic-microscopy data using a single-image super-resolution method

Adrian Basarab, Daniel Rohrbach, Ningning Zhao, Jean-Yves Tourneret, Denis Kouamé, Jonathan Mamou

ENHANCEMENT OF 250-MHZ QUANTITATIVE ACOUSTIC-MICROSCOPY DATA USING A SINGLE-IMAGE SUPER-RESOLUTION METHOD

Adrian Basarab[1]*, Daniel Rohrbach*[2]*, Ningning Zhao*[1]*, Jean-Yves Tourneret*[1]*, Denis Kouamé* [1]*, Jonathan Mamou*[2]

[1] University of Toulouse, IRIT, CNRS UMR 5505, Université Paul Sabatier, INP-ENSEEIHT, Toulouse, France

[2] Lizzi Center for Biomedical Engineering, Riverside Research, New York, NY, USA

{basarab, zhao, tourneret,kouame}@irit.fr, {jmamou, drohrbach}@riversideresearch.org

ABSTRACT

Scanning acoustic microscopy (SAM) is a well-accepted imaging modality for forming quantitative, two-dimensional maps of acoustic properties of soft tissues at microscopic scales. The quantitative maps formed using our custom SAM system using a 250-MHz single-element transducer have a nominal resolution of 7 μm, which is insufficient for some investigations. To enhance spatial resolution, a SAM system operating at even higher frequencies could be designed, but associated costs and experimental difficulties are challenging. Therefore, the objective of this study is to evaluate the potential of super-resolution (SR) image processing to enhance the spatial resolution of quantitative maps in SAM. To the best of our knowledge, this is the first attempt at using post-processing, image-enhancement techniques in SAM. Results of realistic simulations and experimental data acquired from a standard resolution test pattern confirm the improved spatial resolution and the potential value of using SR in SAM.

Index Terms— Scanning acoustic microscopy, quantitative imaging, acoustic properties, single image super-resolution, total variation regularization.

1. INTRODUCTION

Scanning acoustic microscopy (SAM) is a well-accepted imaging modality for forming quantitative, two-dimensional (2D) maps of acoustic properties of soft tissues at microscopic scales [1]. For example, using our custom SAM system which employs a 250-MHz single-element transducer, the resulting 2D acoustic impedance (Z) maps (2DZMs) have a nominal resolution of 7 μm, which is inadequate for some investigations [2]. To enhance resolution, a SAM system operating at even higher frequencies could be designed, but associated costs and experimental difficulties are challenging. Manufacturing transducers operating at 500 MHz or even 1 GHz can be very difficult and associated costs in the transmit receive lines are prohibitive (e.g., A/D card, pulser and receiver). Systems operating at such high frequencies are very sensitive to environmental effects (e.g., vibrations, temperature), and require a very robust design including very precise and expensive motor stages. Therefore, the objective of this study is to evaluate the potential of super-resolution (SR) image processing to enhance 2DZM resolution obtained using our 250-MHz SAM system [2].

Single-image SR is a well-established research field in image processing. It seeks to restore a high-resolution (HR) image from a low-resolution (LR) observed image, *i.e.*, a blurred, decimated and noisy version of the HR image [3]. Reconstruction-based approaches are among the most-popular techniques of SR. They formulate the SR problem as an ill-posed inverse problem and solve it incorporating application-dependent regularization terms. In this paper, the potential of such a reconstruction method [4] to improve the spatial resolution and quality of 2DZMs is investigated.

The remainder of the paper consists of three additional sections. Section 2 summarizes the image-formation model in SAM and formulates the SR in SAM as an optimization problem. Section 3 describes results of simulations and experimental data, and Section 4 presents conclusions.

Part of this work has been supported the CIMI Labex, Toulouse, France, under grant ANR-11-LABX-0040-CIMI within the program ANR-11-IDEX-0002-02.

2. SAM SUPER-RESOLVED IMAGING

2.1. Image formation model

SAM data are acquired by emitting and receiving ultrasound pulses using a single-element transducer while scanning the sample in the (x_1, x_2) plane, perpendicular to the direction of ultrasound wave propagation. Thus, a 3D volume of data is available, which will be denoted hereafter by $\mathbf{y}(x_1, x_2, t)$, where t stands for the time dimension. Acoustic parameters such as impedance (Z), speed of sound, and attenuation are estimated pointwise from each radiofrequency (RF) signal, resulting into 2D quantitative maps existing in the (x_1, x_2) plane. The values of these parameters are computed in this paper using recently proposed estimators described in [2, 5].

Despite the high frequencies employed in SAM, the spatial resolution (in x_1 and x_2 directions) may remain insufficient for specific clinical applications and, as outlined above, improvement by instrumentation techniques is very challenging. In this paper, we model the inadequate spatial resolution, *i.e.,* the image-degradation process, by two blurring and decimation operators and by an additive white Gaussian noise. Let us denote by $\mathbf{y}_t$ the vectorized version, using standard lexicographic order, of one slice from the SAM volume data $\mathbf{y}$ corresponding to time t, where t is an integer between 1 and $N = Tf_s$, with T the time duration of the acquired RF signals and f_s the sampling frequency. The direct model for a given time t can then be written as

$$\mathbf{y}_t = \mathbf{S}\mathbf{H}\mathbf{x}_t + \mathbf{n}_t \tag{1}$$

where the vector $\mathbf{y}_t \in \mathbb{R}^{N_l \times 1}$ ($N_l = m_l \times n_l$) is the measured data at time t, $\mathbf{x}_t \in \mathbb{R}^{N_h \times 1}$ ($N_h = m_h \times n_h$) is the vectorized super-resolved slice to be estimated, with $N_h = d^2 N_l$ (d is an integer representing the super-resolution factor, fixed at 2 in this paper) and $\mathbf{n}_t \in \mathbb{R}^{N_l \times 1}$ is the Gaussian noise. The matrices $\mathbf{S} \in \mathbb{R}^{N_l \times N_h}$ and $\mathbf{H} \in \mathbb{R}^{N_h \times N_h}$ stand for the decimation and blurring (convolu-

tion) operators. $\mathbf{H}$ is a block circulant matrix with circulant blocks (BCCB) modelling the 2D convolution between the super-resolved slice and the point-spread-function (PSF), and left multiplying by $\mathbf{S}$ corresponds to down-sampling with an integer factor d in each spatial direction.

SAM permits forming images in the (x_1, x_2) plane. Therefore, contrary to conventional ultrasound imaging applications, the PSF is not a function of imaging depth. The PSF is spatially invariant in the (x_1, x_2) plane. In fact, a reasonable approximation to the PSF can be obtained from first principles and published equations for spherically-focused transducers in their focal plane [6]. In this work, the PSF is assumed to be known for simulated and experimental data.

2.2. Super-resolution model inversion

To investigate the potential value of SR in SAM imaging, we consider a very recent technique that is more accurate and computationally efficient than several existing methods as shown in our previous studies [4]. Following traditional image-reconstruction problems, the super-resolved slice $\mathbf{x}_t$ (the subscript corresponding to the time variable is omitted in the following) is estimated using a numerical optimization procedure to minimize the following function:

$$\min_{\mathbf{x}} \frac{1}{2}\|\mathbf{y} - \mathbf{SHx}\|_2^2 + \tau\phi(\mathbf{Ax}) \tag{2}$$

where τ is a regularization parameter manually tuned, $\phi(\mathbf{Ax}) = \sqrt{\|\mathbf{D}_\mathrm{h}\mathbf{x}\|^2 + \|\mathbf{D}_\mathrm{v}\mathbf{x}\|^2}$ is the total variation penalization and $\mathbf{A} = [\mathbf{D}_\mathrm{h}, \mathbf{D}_\mathrm{v}]^T \in \mathbb{R}^{2N_h \times N_h}$, with $\mathbf{D}_\mathrm{h}$ and $\mathbf{D}_\mathrm{v}$ standing for horizontal and vertical numerical derivative operators. Note that in this paper we employed the total variation to regularize the solution [7]. The choice was based on the piecewise constant nature of SAM slices. However, exploring other regularization terms is of high interest in SAM and represents an important perspective of this work.

To solve (2), we use a fast algorithm that we described for general image processing applications in [4] and adapted to standard medical ultrasound imaging in [8]. This algorithm is based on a classical implementation of the alternating direction method of multipliers (ADMM) adapted to SR imaging [7]. It presents better convergence properties due to an efficient implementation of the ℓ_2-ℓ_2 problem solution, as explained in detail in [4]. In order to use the ADMM framework, the problem (2) is rewritten in its constrained form as

$$\begin{aligned} \min_{\mathbf{x},\mathbf{u}} \quad & \frac{1}{2}\|\mathbf{y} - \mathbf{SHx}\|_2^2 + \tau\phi(\mathbf{u}) \\ \text{subject to} \quad & \mathbf{Ax} = \mathbf{u}. \end{aligned} \tag{3}$$

The associated augmented Lagrangian (AL) is

$$\mathcal{L}(\mathbf{x}, \mathbf{u}, \boldsymbol{\lambda}) = \frac{1}{2}\|\mathbf{y} - \mathbf{SHu}\|_2^2 + \tau\phi(\mathbf{u}) + \frac{\mu}{2}\|\mathbf{Ax} - \mathbf{u} + \boldsymbol{\lambda}\|_2^2 \tag{4}$$

where $\boldsymbol{\lambda}$ is the scaled dual variable updated at each iteration and μ is a manually tuned hyperparameter. For a given iteration k, the SR algorithm consists of three steps

$$\mathbf{x}^{k+1} = \underset{\mathbf{x}}{\operatorname{argmin}} \|\mathbf{y} - \mathbf{SHx}\|_2^2 + \mu\|\mathbf{Ax} - \mathbf{u}^k + \boldsymbol{\lambda}^k\|_2^2 \tag{5}$$

$$\mathbf{u}^{k+1} = \underset{\mathbf{u}}{\operatorname{argmin}} \tau\phi(\mathbf{u}) + \frac{\mu}{2}\|\mathbf{Ax}^{k+1} - \mathbf{u} + \boldsymbol{\lambda}^k\|_2^2 \tag{6}$$

$$\boldsymbol{\lambda}^{k+1} = \boldsymbol{\lambda}^k + (\mathbf{Ax}^{k+1} - \mathbf{u}^{k+1}). \tag{7}$$

While the variable $\mathbf{u}$ is updated using the Moreau proximity operator, $\mathbf{x}$ is estimated through the analytical solution adapted to high-dimensional images described in [4].

The SR reconstruction is processed independently slice by slice, for each time t, resulting into a super-resolved SAM volume $\mathbf{X}$. This data volume is further used as input for the acoustic-parameter estimators [2,5], providing SR 2D quantitative maps. Note that SR could also be applied directly to the quantitative maps estimated from the raw data. However, the gaining access to the PSF would be far more challenging, because of the non-linearity of the estimators.

3. RESULTS

The feasibility of post-processing SR in SAM is discussed here in terms of simulated and experimental data acquired from a resolution target. Using the simulation data, SR performance is quantified by three standard metrics: the normalized root mean square error (NRMSE), the peak signal-to-noise ratio (PSNR) and the improved signal-to-noise ratio (ISNR), defined as follows.

$$\mathrm{NRMSE} = \sqrt{\frac{\|\mathbf{x} - \hat{\mathbf{x}}\|^2}{\|\mathbf{x}\|^2}}, \mathrm{PSNR} = 10\log_{10}\frac{N_h \max(\mathbf{x})^2}{\|\mathbf{x} - \hat{\mathbf{x}}\|^2}$$

$$\mathrm{ISNR} = 10\log_{10}\frac{\|\mathbf{x} - \bar{\mathbf{y}}\|^2}{\|\mathbf{x} - \hat{\mathbf{x}}\|^2}$$

where the vectors $\mathbf{x}, \bar{\mathbf{y}}, \hat{\mathbf{x}}$ are the ground truth HR image, the bicubic interpolated LR image and the restored SR image respectively. The value of $\max(\mathbf{x})$ defines the largest value of $\mathbf{x}$. Note that the ISNR allows quantifying the improvement of the SR algorithm compared to bicubic interpolation.

The absence of ground truth for the experimental data does not allow the evaluation of SR results with the same metrics. Therefore, the visual inspection of the results will allow the reader to evaluate the spatial-resolution improvement.

3.1. Simulated data

3.1.1. Simulation setup

To evaluate the performance of the SR approach, simulations were conducted that required a reference signal $s_0(t - t_0)$. To mimic experiments closely, we chose to use an experimentally measured reference signal, which was digitized at 2.5 GHz with 12 bit accuracy. Simulations consisted of prescribing values for tissue thickness (Th), speed of sound (c), acoustic impedance Z, and acoustic attenuation (α) as a function of frequency for every pixel in the (x_1, x_2) plane.

A photomicrograph of an H&E-stained histology section (see Fig. 1(a)) was digitized at 20X (i.e., 0.48 μm per pixel). Then, the values of acoustic parameters were linearly assigned depending on the color component of each pixel in the image. The values were varied in a realistic range: c varied between 1400 and 1826 m/s, Z varied between 1.55 and 1.85 MRayl, α was kept constant at 0.86 dB/MHz/cm, and Th was also kept constant and equal to 12 μm. One RF signal, $s^{\mathrm{Sim}}(t)$, was generated for each (x_1, x_2) pixel of the original histology image. This process generated a 3D block of data $\mathbf{y}(x_1, x_2, t)$ by summing the two modified versions of the reference signal (reflections at interfaces involving water and glass, respectively) obtained from the values of Th, c, Z, and α at each pixel location position

$$s^{\mathrm{Sim}}(t) = C_1 s_0(t - t_1) + C_2 s_0^*(t - t_2), \tag{8}$$

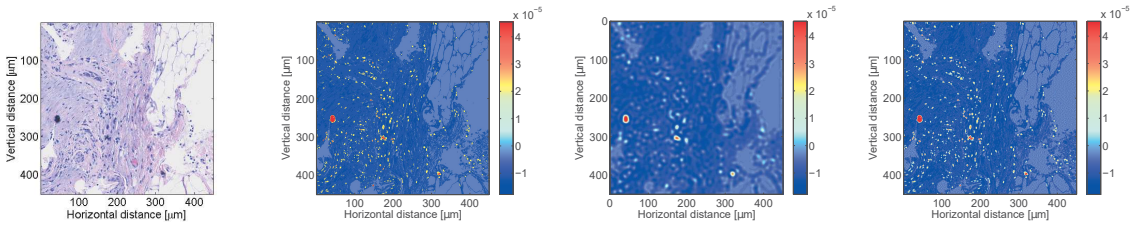

(a) Histology (b) HR slice (c) LR slice (d) SR slice

Fig. 1. Simulation result from a histology section (a) showing one (x_1, x_2) slice extracted from (b) the true high-resolution (HR), (c) the observed low-resolution (LR) and (d) the estimated super-resolved (SR) data volumes. Note that the LR slice has been scaled for better visualization in this figure (*i.e.*, the actual LR slice contains 4 times fewer pixels than the corresponding HR and SR slices. Pixel values represent the amplitude (V) of the RF signals for $t = 200$.

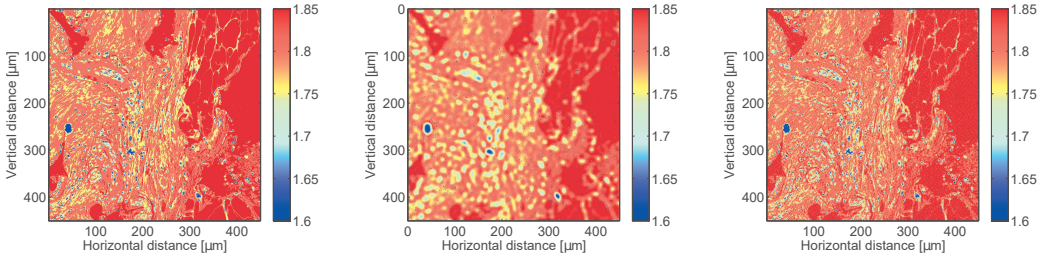

(a) HR impedance map (b) LR impedance map (c) SR impedance map

Fig. 2. Simulation result showing impedance maps in MRayl estimated using (a) the true high-resolution (HR), (b) the observed low-resolution (LR) and (c) the estimated super-resolved (SR) data volumes. Note that the LR impedance map has been scaled for better visualization in this figure (*i.e.*, the actual LR map contains 4 times fewer pixels than the corresponding HR and SR maps.

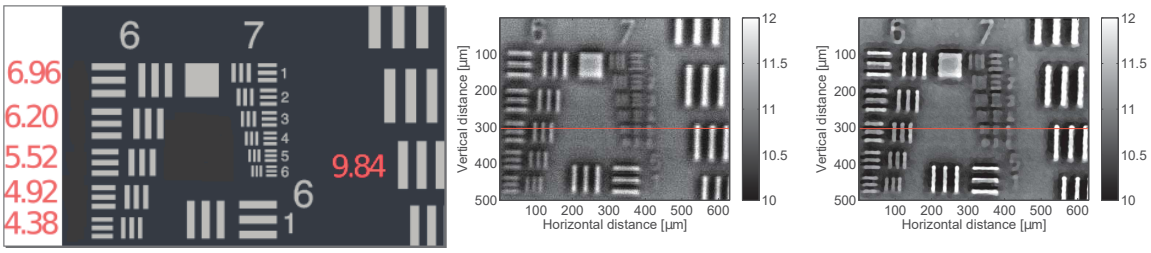

(a) USAF 1951 resolution test chart (b) LR impedance map (c) SR impedance map

Fig. 3. Impedance maps estimated from (b) the original and (c) the super-resolved RF volume acquired on the USAF 1951 resolution test chart (cartoon image shown in (a)). Note that the LR impedance map has been scaled for better visualization in this figure (*i.e.*, the actual LR map contains 4 times fewer pixels than the corresponding SR map. The red numbers in (a) indicate the width in μm (equal to the pitch) between the bars.

where

$$t_1 = t_0 + \frac{2Th}{c_w}, t_2 = t_0 + \frac{2Th}{c} - \frac{2Th}{c_w} \quad (9)$$

$$C_1 = \frac{Z - Z_w}{Z + Z_w}\frac{Z_g + Z_w}{Z_g - Z_w}, \quad (10)$$

$$C_2 = \frac{2Z}{Z_w + Z}\frac{Z_g - Z}{Z_g + Z}\frac{2Z_w}{Z_w + Z}\frac{Z_w + Z_g}{Z_w - Z_g}, \quad (11)$$

where c_w and Z_w are the known speed of sound and acoustic impedance of water, and Z_g is the known acoustic impedance of glass obtained from first principles. The '*' symbol in (8) symbolizes acoustic attenuation effects which are applied in the frequency domain.

Finally, to appropriately simulate the effect of the PSF on the data, at each time depth of the 3D block of data, the 2D slices were convolved by the theoretical PSF of our 250-MHz transducer, generated using a Bessel function with a f-number equal to 1.16 [6]. Each slide was then undersampled by a factor of 2 in each spatial direction. In these simulations, we formed noise-free HR slices with 1000×1000 pixels (at 0.48 μm per pixel), while the LR slices were decimated to be 500×500 pixels (at 0.96 μm/pixel). Note that the

pixel sizes of the LR and HR slices are still much finer than the theoretical resolution of 7 μm allowed by the 250-MHz SAM system. A total number of 400 time slices with a spacing of 4 ns between adjacent slices (i.e., the sampling frequency was 2.5 GHz) was generated.

3.1.2. Simulation results

Figure 1 shows the simulation results obtained for one of the 400 slices (i.e., at $t = 200$). As expected, the effects of the PSF on spatial resolution are evident when comparing Fig. 1(b) to Fig. 1(c), which allows visual appreciation of the spatial-resolution improvement.

As in Fig. 1, Fig. 2 shows the 2DZMs estimated from the HR, LR, and estimated SR data volumes [2, 5]. Again the resolution improvement is striking. Similar improvements were obtained for the 2D speed of sound maps (results not shown). The numerical values of our quality metrics (see Table 1) confirm the ability of the SR algorithm to recover the HR RF slices (mean and standard deviation values are provided), the HR 2DZM and c maps with high accuracy. Note that PSNR values higher than 38 dB are obtained for the estimated 2DZM and c, which is very promising.

Table 1. Numerical results on simulated data.

	RF volume	Impedance	Speed of sound
NRMSE	0.0777 ± 0.1	0.0121	0.0126
PSNR [dB]	36.1173 ± 13.7	38.53	38.29
ISNR [dB]	5.4092 ± 0.9	7.71	6.81

3.2. Experimental data

3.2.1. Acquisition setup

The 250-MHz SAM system has been described in detail previously [2]. Briefly, the sample is mounted on a slide holder and is raster scanned in 2D using 2 μm step size in x_1 and x_2 directions. At each scan location, the amplified RF signals are digitized with 12-bit accuracy and with a sampling frequency of 2.5 GHz using an oscilloscope. The RF data are processed offline to produce 2D maps of acoustic parameters.

The SAM system typically is used to assess thin section of soft tissues for biomedical-research applications, but for this investigation of SR, a spatial-resolution target was scanned. As shown in Fig. 3(a), the target consists of small bars of known width and spacing. Therefore, it represents an ideal target object to evaluate whether our proposed SR method can improve spatial resolution. Note that because the chrome used to form those bars is deposited using photolithography, the metal thickness (i.e., ~ 0.12 μm) is much smaller than the wavelength at 250 MHz (i.e., ~ 6 μm) and therefore only the acoustic impedance can be estimated and only 2DZMs of the target can be formed.

3.2.2. Experimental results

Figure 3(a) shows a cartoon image of the target used in this experiment, together with the LR and estimated SR 2D impedance maps. One lateral impedance profile extracted at a vertical distance of 300 μm, corresponding to the red line in Fig. 3(a) and (b) is shown in Fig. 4. Visual inspection of the impedance maps as well as the lateral profiles show the improvement in spatial resolution obtained with the proposed method. In particular, the code bars are better defined, as well as the numbers in the central part of the images.

A magnification of the vertical-bar profiles also is displayed in Fig. 4, which clearly shows the flatness of the Z values inside a bar on the SR image compared to the LR image. The true width, in μm between the bars, equal to the space between them, is given by the red numbers in Fig. 3(a). One can appreciate that these values are close to the ones highlighted by the horizontal profile in Fig. 4, extracted from the SR impedance image.

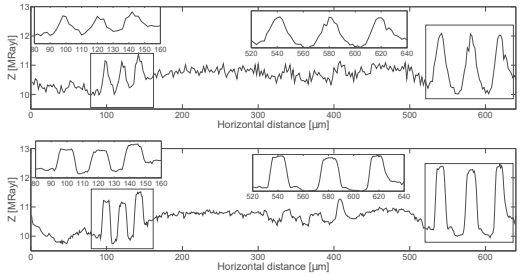

Fig. 4. Horizontal profiles extracted from the LR (up) and SR (down) impedance maps corresponding to USAF 1951 resolution phantom at depth of 300 μm depth (red lines in Fig. 3 and (b)). Two magnifications of the local region corresponding to the code bars are also provided.

4. CONCLUSION

This paper described a study of the effectiveness of single-image SR in SAM. Based on total variation regularization and on a recently proposed ADMM-based optimization technique, the reconstruction algorithm was applied slice by slice in order to estimate data cubes with improved spatial resolution. Simulation and experimental results confirmed the value of using SR in SAM imaging. Further studies will explore other SR methods and regularization terms and their robustness to noise, the automatic estimation of the PSF (blind SR) and the validation of the described method to biological samples using appropriate quantitative metrics.

5. REFERENCES

[1] R. A. Lemons and C. F. Quate, "Acoustic microscopy: biomedical applications," *Science*, vol. 188, no. 4191, pp. 905–11, 1975.

[2] D. Rohrbach, H. O. Lloyd, R. H. Silverman, and J. Mamou, "Fine-resolution maps of acoustic properties at 250 mhz of unstained fixed murine retinal layers," *The Journal of the Acoustical Society of America*, vol. 137, no. 5, pp. EL381–EL387, 2015.

[3] S. C. Park, M. K. Park, and M. G. Kang, "Super-resolution image reconstruction: a technical overview," *IEEE Signal Process. Mag.*, vol. 20, pp. 21–36, 2003.

[4] N. Zhao, Q. Wei, A. Basarab, N. Dobigeon, D. Kouamé, and J.-Y. Tourneret, "Fast single image super-resolution using a new analytical solution for ℓ_2-ℓ_2 problems," *IEEE Trans. Image Process.*, vol. 25, no. 8, pp. 3683–3697, 2016.

[5] D. Rohrbach, A. Jakob, H. Lloyd, S. Tretbar, R. H. Silverman, and J. Mamou, "A novel quantitative 500 mhz acoustic-microscopy system for ophthalmologic tissues," *IEEE Trans Biomed Eng*, 2016, in press.

[6] G. Kino, *Acoustic waves: devices, imaging, and analog signal processing*, ser. Prentice-Hall Signal Processing Series. Prentice Hall PTR, 1987.

[7] M. K. Ng, P. Weiss, and X. Yuan, "Solving constrained total-variation image restoration and reconstruction problems via alternating direction methods," *SIAM J. Sci. Comput.*, vol. 32, pp. 2710–2736, 2010.

[8] N. Zhao, Q. Wei, A. Basarab, D. Kouamé, and J.-Y. Tourneret, "Super-resolution of medical ultrasound images using a fast algorithm," in *Proc. IEEE International Symposium on Biomedical Imaging: From Nano to Macro, Prague*, April 2016, pp. 473–476.